Cation Exchange, Dehydration, and Calcination in Clinoptilolite: In Situ X-ray Diffraction and Computer Modeling

Matthew Johnson,[†] David O'Connor,[‡] Paul Barnes,*[,‡] C. Richard A. Catlow,[†] Scott L. Owens,[§] Gopinathan Sankar,[†] Robert Bell,[†] Simon J. Teat,[||] and Richard Stephenson[†]

The Royal Institution, 21 Albemarle Street, London W1X 4BS, United Kingdom, Department of Crystallography, Birkbeck College, Malet Street, London WC1 E 7HX, United Kingdom, BNFL, Risley, Warrington, Cheshire WA3 6AS, United Kingdom, and CLRC Daresbury Laboratory, Daresbury, Warrington WA4 4AD, United Kingdom

Received: July 19, 2002; In Final Form: October 3, 2002

Clinoptilolite is a natural microporous material possessing a versatile range of cation exchange properties that are exploited in many industrial processes. The dehydration and cation mobility of three prototype forms, Cs−, K−, and Na−clinoptilolite, have been studied using in situ synchrotron energy dispersive and microcrystal diffraction with a novel hybrid simulation technique. This exposes the different responses of the framework, cation, and water components to dehydration processes. The responses are illustrated for the Cs and Na forms using structural snapshots and statistically averaged parameters. The "heat collapse" framework transformation has been identified with the pure Na form by both the in situ diffraction data and the computer modeling.

1. Introduction

Clinoptilolite hails from the heulandite family of zeolites, which shares the same topology of eight- and 10-membered ring channels running parallel to the *c*-axis and an intersecting eight-membered ring channel parallel to the *a*-axis.[1] The defining difference between heulandite and clinoptilolite is the Si/Al ratio, clinoptilolite being assigned if the Si/Al ratio is greater than 4.0.[2,3] The formal charge imbalance between the aluminum tetrahedra (Al^{3+}) and the bridging oxygens (O^{2-}) of the framework brings about a net negative charge, which is counterbalanced by cations, such as Ca^{2+} and Mg^{2+}, in the natural mineral. Clinoptilolite is used in many industrial applications, due primarily to its abundance and cation exchange ability. It is extensively used for the removal of Cs and Sr from low-level waste streams of nuclear power plants,[4] and it is this application that spurred this investigation into the effects of various cations on the structural integrity of clinoptilolite. Many industries use natural Na−clinoptilolite as a trap for radioactive isotopes. However, it is known that the waste streams are typically at temperatures over 100 °C, which can affect the structure of a natural clinoptilolite. Previous work[5,6] has examined the effects of cation type on the unit cell of clinoptilolite over its dehydration range. Smyth et al.[7] studied both natural and Cs-exchanged clinoptilolite single crystals, identifying the cation positions. The dehydration of natural clinoptilolite single crystals (containing predominantly Ca and Na) was studied by Armbruster et al.[8,9] who found a heat-collapsed structure, which was related to Al concentration on the T2 site and cation location; an earlier work by Koyama and Takéuchi[10] had suggested that this collapse was inhibited with K-rich clinoptilolite, and this was also confirmed later by Galli et al.[11] An important aim of this investigation has been to use fully exchanged samples in order to clarify the effect of different cations on the structural changes with temperature, in contrast to studies on mixed cation samples where the attribution is not clearly defined. In particular, we conclusively identify the cause of the heat-collapsed framework structure described in earlier work.

We have examined the behavior of fully exchanged clinoptilolites using a unique combination of diffraction (energy dispersive diffraction, microcrystal diffraction) and computer modeling techniques. These have given a deeper insight into the effect of cation type and water content on the structure and stability of clinoptilolite, and this is illustrated in detail for two prototype monovalent forms, Cs− and Na−clinoptilolite.

2. General Procedures

The experimental and computational studies were based at two nearby sites (The Royal Institution and Birkbeck College, respectively) and carried out in parallel over a three year period (1999−2002). This provided some measure of independence in the analyses of the simulation and experimental data, the convergence between these two only becoming fully apparent after the diffraction data were analyzed in the final stages of the project; the details for these are given in the following sections: 3−5.

Sample preparation and characterization (thermal analysis, electron microscopy) were performed at the two main host sites. Two sources of clinoptilolite were used as follows: For the powder diffraction experiments, the natural clinoptilolite from Mud Hills (California, U.S.A) was selected, based on previous trials[12] of its selectivity for cesium. For the single crystal diffraction measurements, microcrystals were scraped from the surface of a natural mineral sample of clinoptilolite supplied by the (London) Natural History Museum collection. Ion exchanges were performed using aqueous salt solutions (1:1

* To whom correspondence should be addressed. E-mail: barnes@img.cryst.bbk.ac.uk.
[†] The Royal Institution.
[‡] Birkbeck College.
[§] BNFL.
[||] CLRC Daresbury Laboratory.

10.1021/jp021672+ CCC: $25.00
Published on Web 01/04/2003

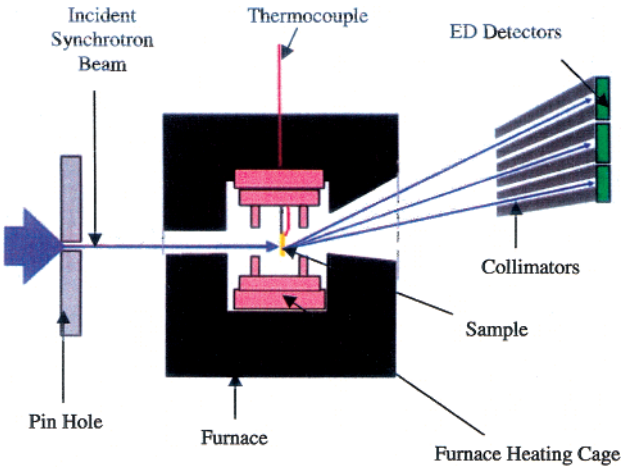

Figure 1. Schematic of the EDD (energy dispersive diffractometer), high-temperature furnace, collimators, and ED detectors.

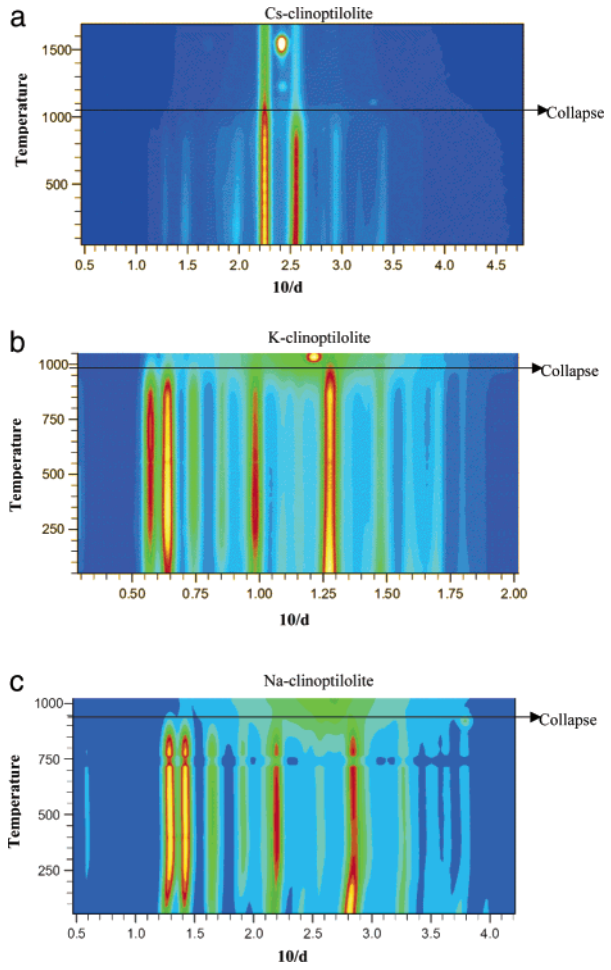

Figure 2. In situ EDD data showing the behavior of (a) Cs−, (b) K−, and (c) Na−clinoptilolite as the temperature is ramped from ambient to 1100 °C at a rate of 5 °C/min, with an EDD pattern collected every 2 min, the detector being set at an angle of 4.986°. The collapse point is indicated, after which the diffraction lines disappear leaving an amorphous band straddled, in the case of panel a, by the Cs fluorescence lines.

mole of salt to clinoptilolite per 10 mL of water) of each cation (e.g., CsCl) for 2 months at room temperature followed by another 2 months in an autoclave at 160−170 °C, the salt solution being renewed weekly. Electron microscope analysis (scanning electron microscopy (SEM) with X-ray fluorescence

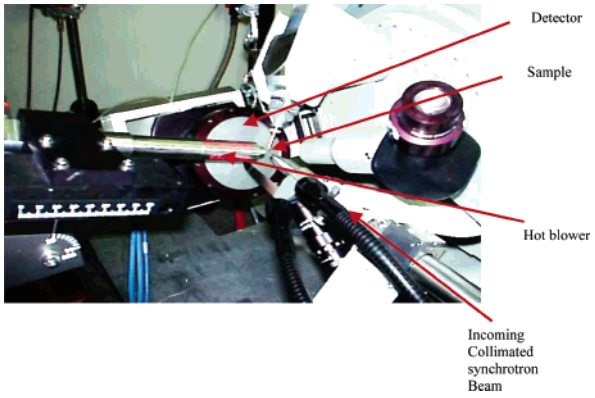

Figure 3. Experimental arrangement for high-temperature single crystal diffraction on station 9.8 at the Daresbury SRS; the essential features are indicated.

microprobe) was used throughout these procedures to test and confirm that the ion exchange had been completed.

3. Energy Dispersive Diffraction

Energy dispersive diffraction is a convenient method for in situ examination of changes in the structure and composition of materials with varying conditions of temperature and pressure, although it is far less useful for structural refinement due to its low diffraction peak resolution and the presence of fluorescence lines. In this study, use has been made of the multiangle[13,14] energy dispersive diffractometer on station 16.4 of the CLRC Daresbury SRS to follow the behavior of exchanged clinoptilolites as they are heated to the point that the framework collapses, with consequent loss of crystallinity. The basic experimental arrangement is shown schematically in Figure 1: An energetic white X-ray beam from a 6 T (synchrotron) wiggler is collimated (typically 1 mm × 1 mm cross-section) and directed into the entrance window of a customized furnace[15] and through a thin (100 mg, 13 mm diameter) pellet of the clinoptilolite sample. A portion (in angle/energy space) of the diffracted X-ray photons passes out through the exit window of the furnace and then further angular selection is effected by means of three collimators placed in front of three energy dispersive (germanium crystal) detectors. Thus, each detector effectively receives a diffraction pattern dispersed in energy. The effective Bragg angle for each collimator−detector unit is determined using calibration samples. In these studies, the most useful data sets were obtained with the middle collimator−detector combination for which the collimator spacing was set at 100 μm with an effective collection angle of 4.986° to the horizontal.

During all of the studies reported here, the furnace was set to operate at a constant ramp rate of 5 °C per minute, starting from ambient conditions and heating to a maximum temperature of 1100 °C (with a calibrated accuracy of ±5 °C). Diffraction patterns were collected every 120 s during heating. The resulting data, for three prototype clinoptilolites, are shown in Figure 2a−c in the form of two-dimensional contour plots. Distinct features are evident for each type and are discussed.

(a) Cs−Clinoptilolite. The patterns consist of diffraction peaks (strongest peaks mainly between 10/d values of 1 and 3.5 Å^{-1}) and the Cs α- and β-fluorescence lines (at positions 2.25 and 2.55 Å^{-1}) corresponding to fluorescence energies of approximately 31 and 35 keV. The diffraction peak positions move only slightly toward shorter d spacings (although this is not obviously visible in Figure 2a) corresponding to an overall reduction in unit cell volume of 2.44(9)% over the refinable

TABLE 1: Atomic Coordinates, Equivalent Isotropic Displacement Parameters (U_{eq} in Å^2), Occupancies, and Unit Cell Parameters for Cs−Clinoptilolite at Three Temperatures (U_{eq} Is Defined as One-Third of the Trace of the Orthogonalized U^{ij} Tensor)[a]

(a) Room Temperature (Full Set)

atom	*x*	*y*	*z*	U_{eq}	partial occupancies
Si(1)	0.21445(8)	0.08889(8)	0.4174(2)	0.015	0.25
Al(1)	0.21445(8)	0.08889(8)	0.4174(2)	0.015	0.75
Si(2)	0.06959(8)	0.20533(8)	0.2151(2)	0.018	
Si(3)	0.21105(8)	0.31151(8)	0.2038(2)	0.018	
Si(4)	0.32274(8)	0.16963(8)	0.2393(2)	0.018	
Si(5)	0.5	0.22135(11)	0.5	0.019	
O(1)	0.1945(4)	0.0	0.4207(11)	0.041	
O(2)	0.1249(3)	0.1314(3)	0.2953(7)	0.041	
O(3)	0.2414(3)	0.3814(3)	0.3546(6)	0.038	
O(4)	0.2776(3)	0.1015(3)	0.3046(7)	0.042	
O(5)	0.1256(3)	0.2757(3)	0.2067(8)	0.047	
O(6)	0.0	0.1839(4)	0.0	0.040	
O(7)	0.0210(3)	0.2251(3)	0.3528(7)	0.047	
O(8)	0.2848(3)	0.2495(2)	0.2630(7)	0.034	
O(9)	0.1906(3)	0.3460(3)	−0.0136(6)	0.039	
O(10)	0.4226(3)	0.1665(3)	0.3790(7)	0.034	
Cs(1)	0.28912(13)	0.5	0.0929(2)	0.091	0.649(3)
Cs(2)	0.4888(15)	0.5	0.045(7)	0.129	0.348(4)
Cs(2A)	0.5129(11)	0.5	−0.0340(10)	0.047	0.348(4)
Cs(3)	0.4472(2)	0.0	0.6046(6)	0.148	0.502(4)
O(3W)	0.5	0.0892(8)	1.0	0.042(3)	=Cs(3)
O(1W)	0.121(3)	0.5	−0.028(6)	0.20(2)	=Cs(1)
O(2W)	0.465(2)	0.434(2)	0.374(5)	0.12(1)	=Cs(2)
unit cell params	$a = 17.4303(6)$ Å,	$\alpha = 90°$,			
	$b = 17.9836(6)$ Å,	$\beta = 113.830(2)°$,			
	$c = 7.4396(3)$ Å	$\gamma = 90°$			
cell volume	2133.21(14) Å^3				
formula weight	2954.04				
calcd density	2.299 g/cm^3				

(b) 200 °C (Cations; No Water)

atom	*x*	*y*	*z*	U_{eq}	partial occupancies
Cs(1)	0.3073(8)	0.5	0.1143(14)	0.073(2)	0.289(8)
Cs(2)	0.4648(9)	0.5	0.0708(15)	0.191(7)	0.132(4)
Cs(3)	0.4352(4)	0.0	0.6200(11)	0.143(4)	0.104(2)
Cs(1A)	0.3137(7)	0.5	0.0898(13)	0.048(2)	0.229(2)
Cs(3A)	0.4694(5)	0.0	0.5544(14)	0.171(6)	0.104(2)
Cs(2A)	0.3379(8)	0.4842(6)	0.112(2)	0.075(3)	0.229(2)
Cs(2B)	0.3883(9)	0.4327(12)	0.171(2)	0.237(9)	0.229(2)
unit cell params	$a = 17.213(6)$ Å,	$\alpha = 90°$,			
	$b = 17.616(6)$ Å,	$\beta = 113.529(9)°$,			
	$c = 7.435(3)$ Å	$\gamma = 90°$			
cell volume	2067.00(13) Å^3				
formula weight	2954.04				
calcd density	2.373 g/cm^3				

(c) 300 °C (Cations; No Water)

atom	*x*	*y*	*z*	U_{eq}	partial occupancies
Cs(1)	0.31584(15)	0.5	0.1056(2)	0.0868(8)	0.594(5)
Cs(1A)	0.3662(8)	0.4583(7)	0.1245(15)	0.148(4)	0.112(3)
Cs(2)	0.4589(12)	0.5	0.084(2)	0.205(9)	0.144(7)
Cs(3)	0.4387(11)	0.0	0.608(3)	0.107(3)	0.174(5)
Cs(3C)	0.4738(8)	0.0	0.546(2)	0.125(4)	0.174(5)
Cs(3A)	0.4290(11)	0.0258(13)	0.676(4)	0.120(4)	0.069(5)
Cs(3B)	0.5	0.087(2)	1.0	0.16(2)	0.053(5)
unit cell params	$a = 17.17(2)$ Å,	$\alpha = 90°$,			
	$b = 17.68(2)$ Å,	$\beta = 113.27(2)°$,			
	$c = 7.456(7)$ Å	$\gamma = 90°$			
cell volume	2080(3) Å^3				
formula weight	2954.04				
calcd density	2.359 g/cm^3				

[a] The full set (framework, cations, and waters) is given for room temperature only since, unlike the cation (Cs) and water (Ow) sites, there are only relatively minor framework changes with temperature. The variations in calculated density derive mainly from the changes in unit cell volume together with the loss of water and cation disorder.

range (50−935 °C), most of this shrinkage, 2.02(7)%, occurring between 50 and 200 °C as water molecules are rapidly lost during dehydration. At ∼1070 °C, the diffraction pattern disappears, corresponding to the collapse of the microporous framework structure, leaving a broad amorphous pattern and the characteristic Cs fluorescence lines.

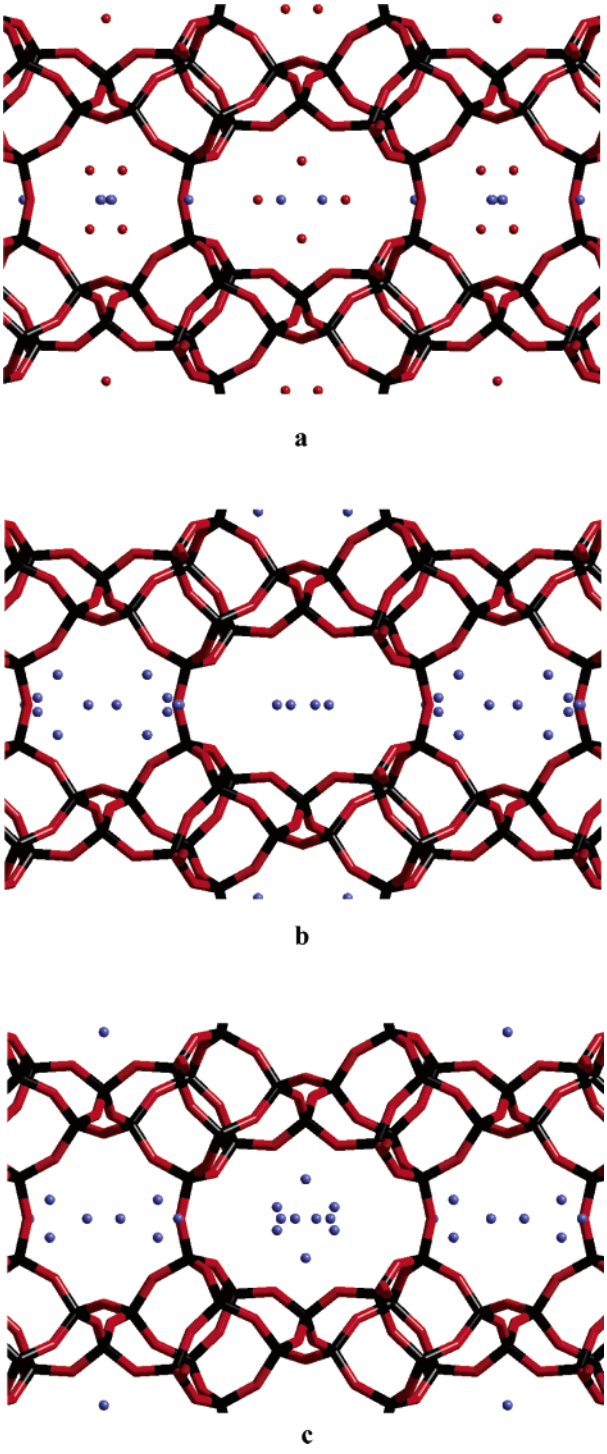

Figure 4. Experimentally determined evolution of Cs (blue spheres) and water (red spheres) positions within the clinoptilolite framework, as viewed down the 001 direction, at (a) 18 (ambient), (b) 200, and (c) 300 °C.

(b) K−Clinoptilolite. The overall picture is similar to Cs−clinoptilolite except that the cation (K) fluorescence peaks are out of range of detection; the diffraction peaks again remain approximately constant, and the structure collapses at a slightly lower temperature of approximately 1000 °C.

(c) Na−Clinoptilolite. The picture here is dramatically different. As with K−clinoptilolite, there is no distinct fluorescence signature; however, the diffraction peaks shift progressively to higher 10/d values between room temperature and 250 °C, after which they remain approximately constant. The eventual collapse is at the noticeably lower temperature of around 920 °C.

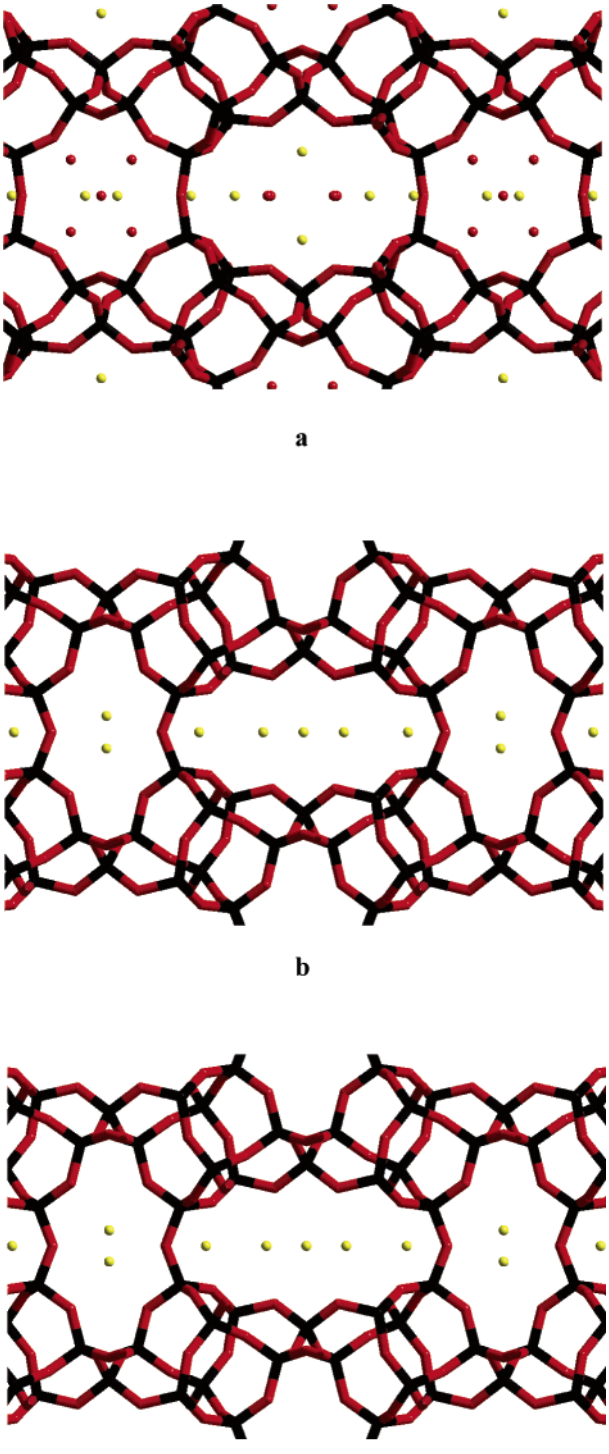

Figure 5. Experimentally determined evolution of Na (yellow spheres) and water (red spheres) positions within the clinoptilolite framework, as viewed down the 001 direction, at (a) 18 (ambient), (b) 200, and (c) 300 °C. The framework transformation between a and b is evident and amplified further in Figure 6.

The preliminary conclusions from the energy dispersive experiments are that the stability of the clinoptilolite framework, as assessed by the temperature of collapse, depends on the cations present, the Cs form being the most stable of the three prototypes chosen and Na−clinoptilolite clearly displays some form of anomalous structural behavior between room and 250 °C—this aspect is revisited later.

4. Microcrystal Diffraction

In situ single microcrystal diffraction measurements were made using the SRS station 9.8 diffractometer[16] (Bruker 1K Smart System). The term microcrystal here refers to crystals less than 100 μm in size, and in these studies, such microcrystals were obtained from the natural clinoptilolite and selected using a polarizing microscope; typical microcrystal dimensions were 35 μm × 35 μm × 5 μm. To reach the required sample temperature, an electrically heated gas stream[17] was directed onto the sample fixed with epoxy resin to a glass fiber, which was also glued to an alumina tube and inserted into the diffractometer goniometer; alumina tubes were chosen because of their low thermal expansion. The temperature using this arrangement (see Figure 3) was controlled to within around ±0.5 °C by means of a thermocouple stationed within 5 mm of the sample, having previously calibrated the temperature offset between the controlling point and the sample. For the three clinoptilolites studied, data collections were carried out at three temperatures, ambient (18 °C), 200, and 300 °C. To ensure that the sample was in equilibrium during each data collection (in terms of both the water content and the temperature), controlled heating/delay periods were designed into the experimental schedule. A typical temperature profile was 4.5 h data collection at 18 °C, ramp from 18 to 200 °C over 3 h, hold steady at 200 °C for 1.5 h prior to data collection, and then repeat this process up to 300 °C, the whole cycle lasting nearly 24 h.

The refinement of the data collected was completed using the WinGX program, which contains the Shelxl-97 routine.[18,19] All refinements were completed in the monoclinic *C*2/*m* space group. The framework bond distances (Si/Al−O) for the refined structures (Tables 1 and 2) average 1.624 Å, all remaining within the 1.582−1.662 Å range. The longest framework bonds are found for the Si(1) site, which was constrained to be the Al site. The O−Si/Al−O framework angles average 109.5° within the range of 104.4−113.4°. The cation sites were assigned on the basis of localized electron densities in the difference Fourier maps, which yield suitable bonding distances to the framework and surrounding water molecules (Cs−O, Cs−H_2O, Na−O, etc.); the occupancies of these sites were then refined as separate variables within the overall refinement. Crystallographic refinement *R* factors (Table 3) for these structures, over the temperature range studied, varied between 4 and 7% in the case of the Na- and K-exchanged clinoptilolites and 6.2−7.2% with Cs−clinoptilolite. The higher *R* factor for Cs−clinoptiolite was a result of the Cs higher electron density showing up a number of disordered cations with very low occupancies, which have proved difficult to model; this disorder can also be perceived in Table 1 from the variations in overall Cs occupancy.

The resultant structural data are summarized in Tables 1 and 2 for the two main cases illustrated in Figures 4 and 5. A description follows on how the cation/water positions change with temperature in terms of three primary cation sites (or regions) that can be identified by viewing down the *001* direction as illustrated in Figures 4 and 5. Site 1: This is at the junction between the small (eight ring) and the large (ten ring) *c* channels and is seen most clearly by viewing down the *001* direction; the site is not always clearly visible when viewing down the *001* channel when it can sometimes be partly hidden at the junction between the small and the large channels. Site 2: This is near the center of the small (eight ring) channel and is clearly visible by viewing down the *001* direction. Site 3: Analogous to site 2, site 3 is near the center of the large (ten ring) channel and is also clearly visible by viewing down the *001* direction.

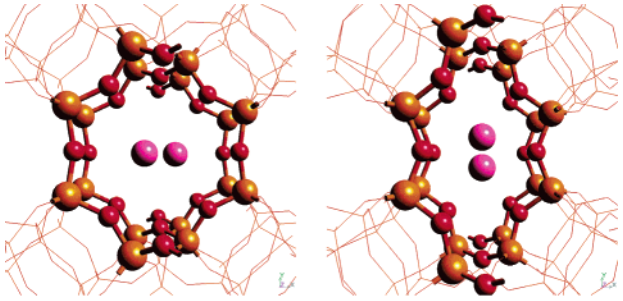

a **b**

Figure 6. Close up view, in the 001 direction, showing the positions of the two Na^+ cations within the eight-membered ring channel before (a) and after (b) the framework transformation.

(a) Cs−Clinoptilolite, 18−300 °C. The evolution from 18 to 300 °C is illustrated in Figure 4. The general tendency with both Cs− and K−clinoptilolite is for the cations to reside on the *020* mirror plane surrounded by their water shells. At 18 °C, the Cs_1 sits very close to the eight ring/ten ring junction so that it is partly hidden in the figure. The Cs_2 site actually comprises two occupancies (Cs_2 and Cs_{2A}) while the Cs_3 site comprises one distinct high occupancy in the largest channel. By 200 °C, the waters are essentially removed and significantly some of the Cs sites move off the *020* mirror plane: the Cs_1 site splits into two (Cs_1, Cs_{1A}), the Cs_2 site splits into three (Cs_2, Cs_{2A}, Cs_{2B}), and the Cs_3 site splits into two (Cs_3, Cs_{3A}). By contrast at 300 °C, there is a reduction in low occupancies at the Cs_2 site but an increase in low occupancy sites in the large channel (Cs_3, Cs_{3A}, Cs_{3B}, Cs_{3C}); however, the trend between 200 and 300 °C is an overall return in Cs density to the *020* mirror plane. There is also an overall unit cell reduction (Table 1b) over the whole temperature range.

(b) K−Clinoptilolite, 18−300 °C. This case is not illustrated, although the pattern of behavior is broadly similar to Cs−clinoptilolite except that the cations (K^+) remain closer to the central *020* mirror plane over the temperature range.

(c) Na−Clinoptilolite, 18−300 °C. The evolution with temperature is dramatically different for this small cation species. The "starting structure" at 18 °C is not unlike those of the Cs and K forms except for the possibility of an additional low occupancy site (Na_4) off the *020* mirror plane reminiscent of Cs−clinoptilolite at 300 °C. By 200 °C, with the water having been essentially removed, the framework has dramatically transformed: this can be seen clearly in Figures 5 and 6 in which the smaller eight ring channel cross-section changes shape such that it becomes more ellipsoidal with the long axis vertical (the *010* direction) while the larger ten ring channel becomes flatter along this direction in compensation. The framework deforms to accommodate these changes, the largest deformation being borne by the Si_1/Al_1-O_1 and Si_2-O_6 bonds. Two obvious consequences of this transformation are that (i) the Na cations in the eight ring channel (the Na_2 site) move off the *020* mirror plane to occupy the extra volume above and below in the *010* direction and (ii) the wider ten ring channel means that the Na_1 site cations now become actual residents of the ten ring channel rather than sitting at the channel junction. This "transformed" situation persists at 300 °C. The unit cell parameters (Table 2) are significantly reduced (by ∼10%) between 18 and 200 °C as the water is lost but increase thereafter to 300 °C. In hindsight, the reason for the anomalous shift in the energy dispersive diffraction data (see Section 3c) now becomes obvious; we interpret these data in terms of a framework transformation, which is completed by around 200 °C and then remains

TABLE 2: As Table 1, Set of Atomic Coordinates, Thermal Parameters (U_{eq}, in Å^2), and Unit Cell Parameters for Na−Clinoptilolite at Three Temperatures[a]

(a) Room Temperature (Full Set)

atom	*x*	*y*	*z*	U_{eq}	partial occupancies
Si(1)	0.28668(5)	0.41043(5)	−0.42241(13)	0.0139(2)	0.25
Al(1)	0.28668(5)	0.41043(5)	−0.42241(13)	0.0139(2)	0.75
Si(2)	0.43308(5)	0.29740(5)	−0.21778(13)	0.0172(2)	
Si(3)	0.29096(5)	0.19030(5)	−0.20184(12)	0.0161(2)	
Si(4)	0.17884(5)	0.32962(5)	−0.23859(13)	0.0165(2)	
Si(5)	0.0	0.28376(7)	−0.5	0.0174(3)	
O(1)	0.3023(2)	0.5	−0.4351(6)	0.0282(8)	
O(2)	0.3805(2)	0.37140(15)	−0.3208(4)	0.0320(6)	
O(3)	0.2668(2)	0.12017(15)	−0.3503(4)	0.0312(6)	
O(4)	0.2324(2)	0.3951(2)	−0.2859(4)	0.0356(7)	
O(5)	0.3728(2)	0.2311(2)	−0.2050(5)	0.0423(8)	
O(6)	0.5	0.3216(2)	0.0	0.0352(9)	
O(7)	0.4861(2)	0.2694(2)	−0.3422(4)	0.0395(7)	
O(8)	0.2124(2)	0.2473(2)	−0.2631(4)	0.0326(6)	
O(9)	0.3134(2)	0.1566(2)	0.0155(4)	0.0364(7)	
O(10)	0.0804(2)	0.33784(15)	−0.3909(4)	0.0302(6)	
Na(1)	0.2781(6)	0.5	0.0465(10)	0.080(3)	0.494(9)
Na(2)	0.4604(3)	0.5	−0.3303(8)	0.061(2)	0.562(6)
Na(3)	0.3321(5)	0.0	−0.1667(9)	0.049(2)	0.444(8)
Na(4)[b]	0.5	0.091(3)	0.0	0.52(3)	0.5
O(1W)	0.5	0.5	0.0	0.063(5)	= Na(1)
O(2W)	0.5742(6)	0.5776(5)	−0.323(2)	0.099(4)	= Na(2)
O(3W)	0.4120(8)	0.0	−0.406(2)	0.077(5)	= Na(3)
O(3AW)	0.430(3)	0.0	0.166(7)	0.24(2)	= Na(3)
unit cell params	a = 17.4030(10) Å,	α = 90°,			
	b = 18.0120(10) Å,	β = 113.812(2)°,			
	c = 7.4350(10) Å	γ = 90°			
cell volume	2132.2(3) Å^3				
formula weight	2294.52				
calcd density	1.787 g/cm^3				

(b) 200 °C (Full Set)

atom	*x*	*y*	*z*	U_{eq}	partial occupancies
Si(1)	0.32117(6)	0.40915(5)	−0.36574(13)	0.0197(2)	0.25
Al(1)	0.32117(6)	0.40915(5)	−0.36574(13)	0.0197(2)	0.75
Si(2)	0.42809(5)	0.26053(5)	−0.21354(12)	0.0215(2)	
Si(3)	0.26115(6)	0.17743(5)	−0.22644(12)	0.0235(2)	
Si(4)	0.18275(5)	0.34557(5)	−0.22108(12)	0.0227(2)	
Si(5)	0.0	0.31142(8)	−0.5	0.0239(3)	
O(1)	0.3601(2)	0.5	−0.3202(5)	0.0329(7)	
O(2)	0.4041(2)	0.35342(14)	−0.2207(4)	0.0423(6)	
O(3)	0.2092(2)	0.11130(15)	−0.3935(3)	0.0371(6)	
O(4)	0.2399(2)	0.4002(2)	−0.3012(4)	0.0424(6)	
O(5)	0.3418(2)	0.2074(2)	−0.2686(4)	0.0494(7)	
O(6)	0.5	0.2372(2)	0.0	0.072(2)	
O(7)	0.4675(2)	0.2454(2)	−0.3736(4)	0.0543(8)	
O(8)	0.19868(14)	0.25089(13)	−0.2343(3)	0.0330(5)	
O(9)	0.2912(2)	0.13085(14)	−0.0140(3)	0.0372(6)	
O(10)	0.07981(14)	0.36816(15)	−0.3572(4)	0.0382(6)	
Na(1)	0.2349(4)	0.0	−0.1461(8)	0.098(2)	0.693(7)
Na(2)	0.5	0.4626(4)	0.0	0.092(3)	0.443(8)
Na(3)	0.0	0.5	−0.5	0.106(6)	0.48(2)
Na(3A)	0.1042(14)	0.5	−0.465(3)	0.055(8)	0.123(8)
unit cell params	a = 16.945(13) Å,	α = 90°,			
	b = 16.876(13) Å,	β = 114.898(12)°,			
	c = 7.369(6) Å	γ = 90°			
cell volume	1912(3) Å^3				
formula weight	2294.52				
calcd density	1.993 g/cm^3				

(c) 300 °C (Cations; No Water)

atom	*x*	*y*	*z*	U_{eq}	partial occupancies
Na(1)	0.2456(3)	0.0	−0.1442(6)	0.094(2)	0.705(7)
Na(2)	0.5	0.4639(5)	0.0	0.111(3)	0.442(8)
Na(3A)	0.0	0.5	−0.5	0.113(5)	0.39(1)
Na(3)	0.099(2)	0.5	−0.461(3)	0.111(6)	0.160(7)
unit cell params	a = 17.009(6) Å,	α = 90°,			
	b = 17.003(5) Å,	β = 114.733(8)°,			
	c = 7.399(2) Å	γ = 90°			
cell volume	1943.5(10) Å^3				
formula weight	2294.52				
calcd density	1.960 g/cm^3				

[a] The full set (framework, cations, and waters) is given for both room temperature and 200 °C in view of the framework transformation occurring within this temperature range. [b] It is not possible to distinguish between this site being a Na cation or water position, which is refined isotropically.

TABLE 3: Basic Refinement Parameters for the Crystallographic Data Given in Tables 1 and 2

Cs−clinoptilolite	20 °C	200 °C	300 °C
θ range for data collection	2.48−28.89°	2.89−29.10°	2.88−29.04°
reflections collected	7149	7100	5256
independent reflections	2888	2836	2749
reflections with $F^2 > 2\sigma$	2174	2035	1911
final R indices ($F^2 > 2\sigma$)	0.069	0.062	0.072

Na−clinoptilolite	20°C	200°C	300°C
θ range for data collection	2.49−28.90°	2.93−29.14°	2.92−28.98°
reflections collected	7196	6433	6598
independent reflections	2900	2610	2629
reflections with $F^2 > 2\sigma$	2286	1873	2019
final R indices ($F^2 > 2\sigma$)	0.052	0.043	0.045

essentially stable until the structure eventually collapses at 920 °C, although the unit cell parameter data indicate some minor reversion back toward the original structure as the temperature approaches 920 °C.

5. Computer Modeling/Simulation

The simulation routines used were a further development of the method of O'Connor et al.[20] in which a combination of constant pressure (NPT) molecular dynamics and energy calculations of individual water molecules are used to conduct simulations for a given temperature profile. These routines were implemented on a Silicon Graphics Octane system using a modified form of the MSI/Accelrys Open Force field module.

The force field used (Table 4) was chosen for a balance of accuracy, transferability, and (computational) simplicity: The valence terms consist of bond (Morse/Harmonic), angle (θ harmonic), and an optional 1−3 term for the framework although the latter was not used to generate the output referred to in this publication. Lennard−Jones (12-6) terms are used for nonbonded extraframework elements and Buckingham (exp-6) terms for more accurate calculations of close framework interactions; van der Waals (VdW) and Coulomb terms are calculated with the Ewald summation. VdW parameters for all framework/ion species are taken from the combined Burchart et al.[21−23] and Universal[24] force-fields; TIP3P[25] charges are used for the water while valence and VdW terms are taken from Dreiding;[26] formal charges are used for the ions (Cs, Na, etc.); the TIP3P and ion charges are constrained, and the framework charges are calculated using the charge equilibration method of Rappe et al.[27] Partial charges are recalculated for the framework after water removal and changes in temperature.

A minimum of two crystallographic unit cells, comprising in excess of 300 atoms, was used as a simulation supercell in order to achieve a representative degree of disorder in the water and ion positions within one complete clinoptilolite cage while still maintaining a computationally feasible simulation program. The initial framework coordinates were taken from the experimental X-ray diffraction data (vide supra), while the water content was introduced by constant volume (NVT) Monte Carlo simulation constrained to fit the experimentally obtained density (thermogravimetric analysis, TGA) at ambient conditions.

An NPT-based simulation procedure was then used for each cation-exchanged clinoptilolite in which the framework, ions, and water molecules are all permitted to move within the described force field, using typically 5×10^4 molecular dynamic steps per temperature point at 10 °C intervals. However, it should be noted that during the early stages of heating the clinoptilolite composition also changes rapidly, losing water molecules during the dehydration stage. A full GCMC (grand canonical Monte Carlo) simulation of this process would be prohibitively long using currently available algorithms, and so a hybrid "dehydration dynamics" method has been devised[28] in which realistic water loss profiles can be incorporated into the simulation. In this method, the potential energy of each water molecule (PE) is calculated and compared with its average kinetic energy (KE) at the current temperature and a probability of removal p is calculated, where

$$p \propto \exp\left(\frac{|\mathrm{KE}| - |\mathrm{PE}|}{k_B T}\right)$$

If $|\mathrm{PE}| > |\mathrm{KE}|$, then p is compared with a random number R (between 0 and 1) and if $p > R$ the molecule is removed. The temperature of the simulation is then increased, and a new set

TABLE 4: List of Potentials Expressed in Units of kcal/mol (Energy), Degrees (for Angles), and Å (Distances)[a]

Framework Bonds (Morse[21−23])

$E_b = D_0(e^{-\sigma(r - r_0)} - 1)^2 - S$, where $\sigma = (K_b/2D_0)^{1/2}$

		D_0	r_0	K_b	S
Si	O	526.00	1.5910	106.9158	106.920
Al	O	545.23	1.7300	109.7583	109.755

Water Bond (Harmonic[26])

$E_b = K_o(r - r_0)^2$

		K_0	r_0
O	H	700.00	0.9800

Framework Three Body (Harmonic[26])

$E_{angle} = K_o(r - r_0)^2$

			K_o	r_0
Si	O	Si	190.610	3.08
Al	O	Si	177.568	3.22
O	Si	O	137.390	2.60
O	Al	O	53.1900	2.83

van der Waals

Lennard−Jones (LJ[26,28])

$$E_{LJ} = D_0\left[\left(\frac{r_0}{r}\right)^{12} - 2\left(\frac{r_0}{r}\right)^6\right]$$

Buckingham (Buck[21−23])

$$E_{exp-6} = D_0\left\{\left(\frac{6}{s-6}\right)e^{s(1-r/r_0)} - \left(\frac{s}{s-6}\right)\left(\frac{r_0}{r}\right)^6\right\}$$

		type	r_0	D_0	s
H (water)	H (water)	LJ	3.195	0.0152	
O (water)	O (water)	LJ	3.405	0.0957	
Ca	Ca	LJ	3.399	0.2380	
Cs	Cs	LJ	4.517	0.0450	
K	K	LJ	3.812	0.0350	
Mg	Mg	LJ	3.021	0.1110	
Na	Na	LJ	2.983	0.0300	
Al	Al	Buck	4.240	0.0292	12.5
O (frame)	O (frame)	Buck	3.300	0.1648	12.5
Si	Si	Buck	4.200	0.4690	12.5
Si	O (frame)	Buck	3.750	0.0841	12.5
Al	Al (frame)	Buck	3.770	0.0659	12.5

[a] The van der Waals entries indicate the pair of species involved, differentiating between oxygens on water molecules ("water") or on framework sites ("frame"); other pair combinations are formed by the geometric (mean) rule. Framework partial charges are assigned by the charge equilibration method;[27] TIP3P[25] charges are applied to the water molecules and formal charges to the ions with a screening (dielectric) constant of 4. The transformation results described could be obtained both using and omitting the framework three body terms, although the best agreement with experimental data was obtained in the latter case.

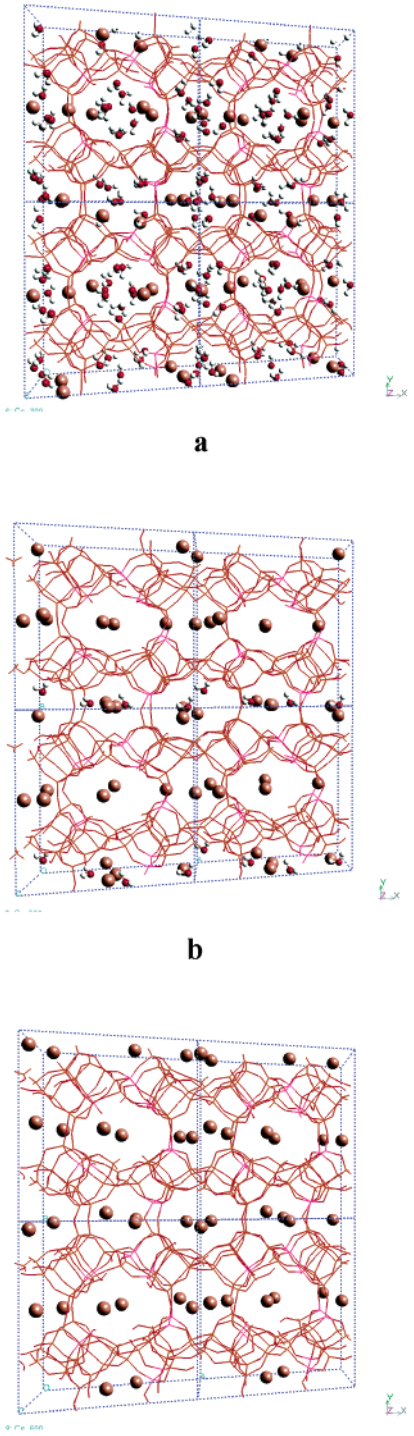

Figure 7. Computer simulation snapshots showing evolution of Cs (brown spheres) and water (red/white spheres) positions within the clinoptilolite framework, as viewed down the 001 direction, at (a) 293 (ambient), (b) 500, and (c) 600 K. The crystallographic unit cells are marked in blue.

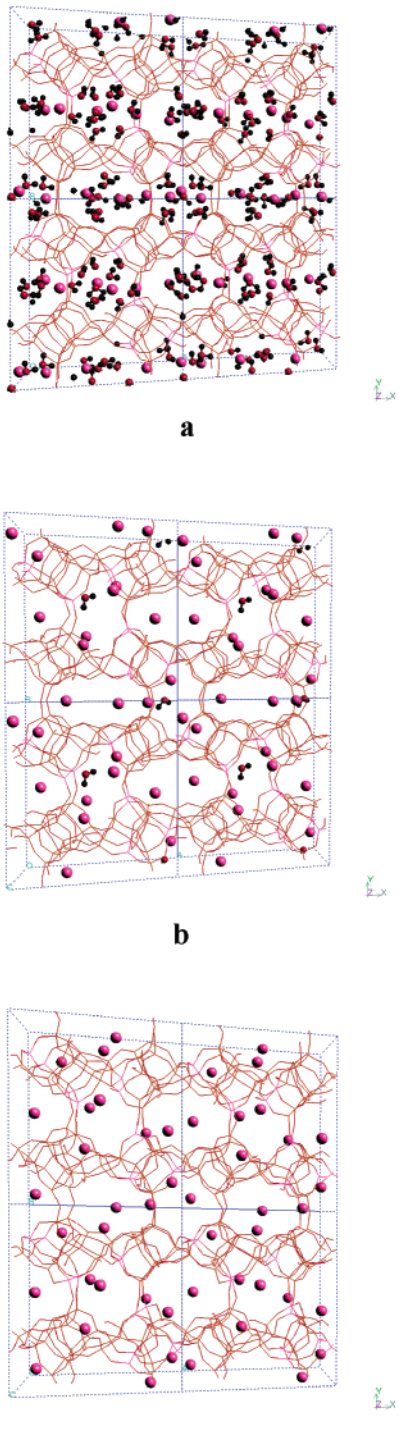

Figure 8. Computer simulation snapshots showing evolution of Na (purple-pink spheres) and water (red/black spheres) positions within the clinoptilolite framework, as viewed down the 001 direction, at (a) 293 (ambient), (b) 500, and (c) 600 K. The crystallographic unit cells are marked in blue. The experimental framework transformation is reproduced between a and b.

of velocities are assigned to the remaining water molecules to satisfy the Maxwell distribution at that temperature. This method is found[28] to reproduce (average of $<5\%$ deviation between the simulated and the measured water weight loss) the weight loss curves obtained by TGA on Cs− and Na−clinoptilolites. With this technique, dehydration simulations could be completed within realistic time periods, typically within 24−96 h for 10^4−10^5 steps per temperature point. Once all of the water has been removed, the simulation reverts to the standard NPT format.

Such simulations generate a large data output, which has to be digested. The main conclusions from this are illustrated by Figures 7−9 for the two extreme cases of Cs− and Na− clinoptilolite. Figures 7 and 8 show simulation snapshots, which can be directly compared with the results from microcrystal diffraction (Figures 4−6). The main structural features evinced from the experimental data (preponderance of cations around the mirror (*020*) plane, pattern of water loss during dehydration,

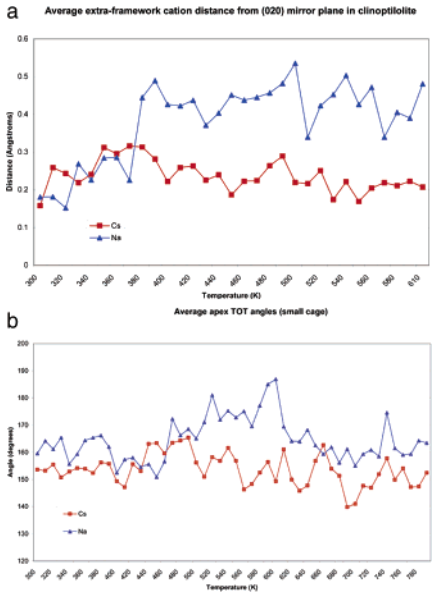

Figure 9. Distribution of geometric parameters for Cs- (■) and Na- (▲) exchanged clinoptilolite against temperature: (a) average cation distance from the 020 mirror plane; (b) average apex TOT angle in the eight-membered ring cage. These parameters, respectively, indicate the proximity of cations to the mirror and give a measure of the state of the eight ring channel. In the case of the Na−clinoptlolite, these parameters change notably above 370 and 450 K, respectively, clearly relating to the cause and effect of the framework transformation.

cell shrinkage, framework transformation in the case of Na−clinoptilolite) are evident even in such isolated snapshots. However, a clear advantage with simulation data is that one can examine structural trends in finer statistical detail and over smaller temperature increments: For example, the dehydration process can be observed down to levels lower than those at which experimental electron densities can be safely assigned to partial water occupancies; thus, the dehydration is found to start in the major ten-membered ring channels whereas the most tightly bound waters, in the small cages as well as locations that screen close cation−cation and cation−framework interactions, persist to above 200 °C in keeping with experimental TGA data. Similarly, the cation−framework interactions can be followed in finer detail than the coarse 100 or 200 °C experimental steps. In Figure 9a, the average modular distance of the mobile cations from the *020* mirror plane is traced throughout the dehydration simulation. This shows that for Cs−clinoptilolite the Cs cations remain on average close (within 0.3 Å) to the *020* mirror plane throughout the simulation, although, in keeping with the experimental trend, the excursions away from this midplane are greatest at the intermediate temperatures (75−150 °C), reducing as the temperature increases above 200 °C. The pattern with Na−clinoptilolite is markedly different, showing a far more abrupt increase, just above 100 °C, of the average Na distance from the midplane. This effect is obviously related to the framework transformation discussed in which the Na_2 site distinctly occupies above and below midplane positions inside the transformed eight ring channel. Figure 9b monitors the small cage apex TOT angle as a (partial) indicator of the state of the eight ring channel, although one notes that this tends to understate the degree of transformation, which involves a change in both the TOT angle and the precessional movement of the TOT plane. Nevertheless, comparison of Figure 9a,b suggests that the framework transformation follows the Na cation readjustment and is completed by around 200 °C after which the higher apex angle remains to well beyond the last experimental measurement (300 °C). Between 300 and 500 °C, Figure 9b suggests that there might be some limited movement of the framework back toward the room temperature structure as thermal motion anneals out some of the lattice strain prior to eventual collapse around 920 °C.

Thus, the contrasting behavior of Na and Cs cations in clinoptilolite is evident from both the experimental and the simulation data. The clinoptilolite structure presents suitable initial space, within the eight ring and ten ring channels centered on the *020* mirror, to accommodate either the Na or Cs cations in the fully hydrated state. During dehydration, the water being transported out of the structure disturbs this spatial equilibrium and this is evident in Figure 9a, which shows the average distance from the mirror plane increasing significantly for both cations as the temperature approaches 100 °C. After the water is removed, the driving force on the cations toward the *020* mirror plane is a combination of the symmetric electrostatic interactions across the plane, which are no longer shielded by intervening water molecules, together with the van der Waals repulsion from the inside of the channel framework. The balance in the case of the much larger Cs cation is such that freedom away from the mirror plane is highly restricted and, unlike the smaller Na cation case, the large perturbations necessary for the promotion of framework transformations do not occur.

6. Conclusions

The main conclusions from this study are as follows.

X-ray diffraction data can be collected routinely under true in situ conditions using both the rapid temperature-resolved low-resolution (energy dispersive) and the fixed temperature high-resolution (single crystal, monochromatic) modes. This combination gives greater confidence regarding structure−temperature relationships of the material under study.

We have obtained essential agreement between the experimental diffraction data and the simulation/modeling output on the behavior of the three main components (water behavior, cation positions, framework structure) for an important microporous material. This suggests that we are reaching the point where simulation can now be considered to be a realistic screening tool for exploring the behavior of different cation combinations.

The structural behavior during dehydration and increasing temperature varies considerably with cation: All cations tend to distribute themselves close to the *020* mirror plane, which bisects the eight ring and ten ring channels running in the *c*-direction, whereas with Na−clinoptilolite greater excursions (higher occupancy) from this midplane occur above 100 °C.

With Na−clinoptilolite, the framework exhibits a clear transformation by 200 °C in which the eight ring channel elongates in the *b*-direction, becoming ellipsoidal, while the larger ten ring channel becomes flatter along this direction in compensation.

The changed shape of the eight ring channel is promoted by the migrating Na cations, which then fit the transformed shape more easily by adopting positions above and below the *020* mirror plane. This effect is a direct consequence of dehydration coupled with the size and mobility of the Na cation and is not found with the other monovalent cations, K and Cs.

The various ion-exchanged clinoptilolites show different stabilities as measured by the temperatures at which the crystalline frameworks collapse. Na−clinoptilolite is the least stable form studied, collapsing at 920 °C; this behavior can now be reconciled in terms of the change in shape of the main structure-reinforcing unit (the cation-filled ten ring channel) and

the framework strain that has to be accommodated in the eight ring channel after transformation.

Acknowledgment. We thank the U.K. research Council (EPSRC) for funding, the CLRC Daresbury Laboratory for synchrotron beam time, the ULIRS (University of London Inter-Collegiate Research Services) for thermal analysis by Dr. M. Odlyha, Birkbeck College for electron microprobe facilities provided by Dr. A. Beard, and University College London, through Prof. G. D. Price, for use of geological facilities.

References and Notes

(1) Merkle, A. B.; Slaughter, M. *Am. Mineral.* **1960**, *53*, 1120.
(2) Mason, B.; Sand, L. B. *Am. Mineral.* **1968**, *45*, 341.
(3) Boles, J. R. *Am. Mineral.* **1972**, *57*, 1452.
(4) Mumpton, F. A. In *Natural Zeolites: Occurrence, Properties, Use*; Sand, L. B., Mumpton, F. A., Eds.; Pergamon: New York, 1978; p 3−27.
(5) Bish, D. L. *Clays Clay Miner.* **1984**, *32*, 444.
(6) Bish, D. L. In *Occurrence, Properties, and Utilization of Natural Zeolites*; Kallo, D., Sherry, H. S., Eds.; Akademiai Kiado: Budapest, 1988; pp 565−576.
(7) Smyth, J. R.; Spaid, A. T.; Bish, D. L. *Am. Mineral.* **1990**, *75*, 522.
(8) Armbruster, T.; Gunter, M. E. *Am. Mineral.* **1991**, *76*, 1872.
(9) Armbruster, T. *Am. Mineral.* **1993**, *78*, 260.
(10) Koyama, K.; Takéuchi, Y. *Z. Kristallogr.* **1977**, *145*, 216.
(11) Galli, E.; Gottardi, G.; Mayer, H.; Preisinger, A.; Passaglia, E. *Acta Crystallogr.* **1983**, *B39*, 189.
(12) O'Neill, L. *Internal BNFL Report ILWET(95)*, April 1996, 59.
(13) Barnes, P.; Jupe, A. C.; Colston, S. L.; Jacques, S. D. M.; Grant, A.; Rathbone, T.; Miller, M.; Clark, S. M.; Cernik, R. J. *Nucl. Instrum. Methods Phys. Res.* **1998**, *B134*, 310.
(14) Muncaster, G.; Davies, A. T.; Sankar, G.; Catlow, C. R. A.; Thomas, J. M.; Colston, S. L.; Barnes, P.; Walton, R.; O'Hare, D. *Phys. Chem. Chem. Phys.* **2000**, *2*, 3523.
(15) Barnes, P.; Jupe, A. C.; Jacques, S. D. M.; Colston, S. L.; Cockcroft, J. K.; O'Connor, D.; Johnson, M.; Catlow, C. R. A.; Bell, R.; Hooper, D. *J. Res. Natl. Inst. Stand. Technol.* Submitted for publication.
(16) Cernik, R. J.; Clegg, W.; Catlow, C. R. A.; Bushnell-Wye, G.; Flaherty, J. V.; Greaves, G. N.; Hamichi, M.; Burrows, I.; Taylor, D. J.; Teat, S. J. *J. Synchrotron Radiat.* **1997**, *4*, 279.
(17) Muncaster, G.; Sankar, G.; Catlow, C. R. A.; Thomas, J. M.; Bell, R. G.; Wright, P. A.; Coles, S.; Teat, S. J.; Clegg, W.; Reeve, W. *Chem. Mater.* **1999**, *11*, 158.
(18) Farrugia, L. J. *J. Appl. Crystallogr.* **1990**, *32*, 837.
(19) Sheldrick, G. M.; *Shelxl-97 Program*; University of Gottingham: Germany, 1997.
(20) O'Connor, D.; Barnes, P.; Bates, D. R.; Lander, D. F. *Chem. Commun.* **1998**, 2527.
(21) Burchart, E. de Vos; Verheij, V. A.; van Bekkum, H.; van de Graaf, B. *Zeolites* **1992**, *12*, 183.
(22) de Vos Burchart, E. Ph.D. Thesis, Delft University of Technology, The Netherlands, 1992.
(23) de Vos Burchart, E.; van Bekkum, H.; van de Graaf, B. *J. Chem. Soc., Faraday Trans.* **1992**, *88*, 1161.
(24) Rappé, A. K.; Casewit, C. J.; Colwell, K. S.; Goddard, W. A., III; Skiff, W. M. *J. Am. Chem. Soc.* **1992**, *114*, 10024.
(25) Jorgensen, W. L.; Chandrasekhar, J.; Madura, J. D.; Impey, R. W.; Klein, M. L. *J. Chem. Phys.* **1983**, *79*, 926.
(26) Mayo, S. L.; Olafson, B. D.; Goddard, W. A., III. *J. Phys. Chem.* **1990**, *94*, 8897.
(27) Rappé, A. K.; Goddard, W. A., III. *J. Phys. Chem.* **1991**, *95*, 3358.
(28) O'Connor, D.; Barnes, P.; Catlow, C. R. A. Manuscript in preparation.